APPLIED SCIENCES AND ENGINEERING

Diagnosing Parkinson's disease via behavioral biometrics of keystroke dynamics

Trinny Tat†, Guorui Chen†, Jing Xu, Xun Zhao, Yunsheng Fang, Jun Chen*

Parkinson's disease (PD) is one of the rapidly growing neurodegenerative diseases, affecting more than 10 million people worldwide. Early and accurate diagnosis of PD is highly desirable for therapeutic interventions but remains a substantial challenge. We developed a soft, portable intelligent keyboard leveraging magnetoelasticity to detect subtle pressure variations in keystroke dynamics by converting continuous keystrokes into high-fidelity electrical signals, thus enabling the quantitative analysis of PD motor symptoms using machine learning. Relying on a fundamental working mechanism, the intelligent keyboard demonstrates highly sensitive, intrinsically waterproof, and biocompatible properties, with the successful demonstration in a pilot study on patients with PD. To facilitate the potential continuous monitoring of PD, a customized cellphone application was developed to integrate the intelligent keyboard into a wireless platform. Together, the intelligent keyboard system's compelling properties position it as a promising tool for advancing early diagnosis and facilitating personalized, predictive, preventative, and participatory approaches to PD healthcare.

INTRODUCTION

Parkinson's disease (PD) affects more than 10 million people globally, costing a total economic burden of $52 billion (*1*). This troubling statistic is exacerbated by the currently incurable nature of the disease, as there are no treatments that can halt or reverse its progression. This not only affects those diagnosed with PD but also places a substantial strain on caregivers. Correspondingly, on the one hand, the severity of PD can lead to faster clearance of medication, such as levodopa, from the bloodstream, reducing the duration of symptom stabilization (*2*). On the other hand, while currently on-the-market PD medications do provide some symptomatic relief, their efficacy diminishes as the disease advances, frequently accompanied by considerable and occasionally intolerable side effects (*3*). Moreover, considering the prevalence of polypharmacy—the use of multiple medications—among the elderly and those with PD (*4*, *5*), to prevent an even greater risk of adverse drug reactions, diagnosing and monitoring PD become crucial interventions to efficiently manage the disease and optimize personalized drug pharmacodynamic properties, which ultimately aim to minimize the side effects on patients and enhance clinical efficacy (*6*).

The current assessment of PD progression heavily relies upon expensive and cumbersome invasive scans, as well as subjective clinical evaluation. For example, the Movement Disorder Society–Unified Parkinson's Disease Rating Scale (MDS-UPDRS) performed by physicians can be subjective, as patients provide their opinions on current symptoms and functional limitations (*7*). Moreover, the MDS-UPDRS is typically administered only during the initial assessment and does not conveniently reflect patients' ongoing status (*8*). On top of that, the assessment may lack objectivity, sensitivity, and repeatability in scale to detect subtle changes (*9*, *10*). Neuroimaging and sonography are alternative and additional approaches that provide high degrees of sensitivity and specificity for early PD confirmation (*11*, *12*). Unfortunately, these nonmotor diagnostic tests require a third-level medical referral, starting from a family practitioner to more specialized physicians such as a neurologist and a neuroimaging specialist (*13*), and, in general, are expensive and intermittent, and unsuitable for frequent and continuous tracking of PD progression. In addition, relying solely on scans cannot effectively confirm PD but rather requires a combination of consultations and examinations (*14*). Worse, there exist some possible adverse reactions such as headache, nausea, vertigo, dry mouth, dizziness, hypersensitivity reaction, and pain (*15*). Consequently, the absence of efficient, quantitative, continuous, and easily accessible biomarkers to track PD progression remains a notable challenge, in both drug development and therapeutic interventions.

In general, patients with PD can exhibit symptoms that visibly affect movements of the hands and fingers (*16*, *17*), such as bradykinesia, tremor (4 to 6 Hz) (*18*, *19*), and rigidity (*20*, *21*), which could alter an individual's keystroke dynamics—the typing patterns on a keyboard (*22*). The reasons for using a keyboard for PD diagnosis are, first, they are widely adopted for human-computer interfacing (*23*), including those with mild to moderate motor impairments, thus making the analysis of keystroke dynamics easily accessible for monitoring typing behavior among patients with PD (*24*, *25*). Second, typing is a common activity that requires fine motor skills and coordination and its quantitative data can be provided via keystroke dynamics. Last, the keyboard can also capture biomarkers, such as flight time (FT), hold time (HT), and force, that reflect motor changes associated with PD (*26*, *27*). Consequently, this device, when designed with such parameters in mind, holds promise in diagnosing PD and, in the future, determining the effectiveness of therapies in slowing disease progression.

Until now, diagnosing PD symptoms using keystroke dynamics has been explored in previous studies (*25*, *26*, *28*–*33*). However, these efforts often rely on conventional wired keyboards that lack integrated sensors and do not capture critical data, such as typing pressure. Henceforward, we present an innovative platform, a soft and pressure-sensitive intelligent keyboard system (IKS) for diagnosing PD symptoms. The IKS leverages the giant magnetoelastic effect, enabling the tracing and recording of the behavioral biometrics of keystroke dynamics by converting typing movements into

Department of Bioengineering, University of California, Los Angeles, Los Angeles, CA 90095, USA.
*Corresponding author. Email: jun.chen@ucla.edu
†These authors contributed equally to this work.

high-fidelity electrical signals. This innovation endows the IKS with self-powered, waterproof, biocompatible, and portable sensing capabilities, allowing for wireless and continuous monitoring of both keystroke pressure and timing data. Unlike traditional keyboards, the IKS enables continuous measurement of both the dynamic time intervals between keystrokes and the force applied to each keystroke. These individualized typing and timing signals serve as personalized and easily accessible biomarkers for continuously monitoring person-specific changes over time in PD. The intelligent keyboard holds a strain of up to 140%, Young's modulus of 563 kPa, a frequency range of 0.5 to 10 Hz that is suitable for capturing human motions and PD tremors during typing, a limit of detection as low as 0.25 kPa, a short response time of 4 ms, and a signal-to-noise ratio (SNR) of 34.5 dB. To enhance its capabilities, we developed a mobile application (APP) that integrates with the intelligent keyboard, forming an IKS. During the successful demonstration of the pilot human study, using deep-learning algorithms, the IKS provided a robust analysis of typing patterns from both participants in laboratory settings and patients with PD, which was harnessed for early diagnosis of PD disease symptoms with an average prediction accuracy of 96.97%. Overall, the soft and pressure-sensitive IKS offers an innovative approach for continuous and personalized monitoring of PD symptoms. Its advanced characteristics and analytical capabilities provide valuable insights for clinical assessment, facilitating early intervention and more effective management of PD disease.

RESULTS

Working mechanism

The intelligent keyboard comprises an array of magnetoelastic keys as sensor units connected in parallel to form the completed modern English alphabet, the space bar, and several punctuation marks such as the comma and period. Consisting of a liquid metal fiber fused with a soft magnetoelastic thin film, each key unit of the intelligent keyboard is pressure sensitive and can convert typing motions on the keyboard into local and high-fidelity electrical signals without the need for an external power source, containing both timing and force information for signal-to-function execution. On the basis of the coupling of magnetoelastic effect and magnetic induction (MI), the intelligent keyboard was developed for analyzing signals produced from subtle variations in typing biometrics to reveal important timing and pressure information regarding the patient's disease status (Fig. 1, A and B, and fig. S1). These keystroke-generated electrical signals can be wirelessly shared with physicians remotely, analyzed to extract clinical information, and diagnose PD, enabling real-time monitoring and assessment from anywhere at any time. Because the electrical signals for diagnosis are generated by finger typing, the intelligent keyboard is working in a self-powered manner. In detail, we focused on developing a typing-driven diagnosis mechanism for the fabrication of a flexible, stretchable, and deformable keyboard (Fig. 1C and fig. S2).

Structurally, each key unit holds two components as two functional layers to complete the typing–to–electrical signal conversion. The first component is a soft magnetoelastic composite, also known as the magnetomechanical coupling (MC) layer, which facilitates the typing-to-magnetic conversion process. Figure S3 depicts the formation process of the MC layer. The other component is the conductive liquid metal fiber that embodies the thin film, acting as the MI layer, enabling the magnetic-to-electrical conversion. Last, the elastomer serves as structural support. Micro–computed tomography (micro-CT; Fig. 1D and movie S1) and scanning electron microscope (SEM) images illustrated in fig. S4 reveals the layer of liquid metal and the soft magnetoelastic thin film with a random distribution of micromagnets in the porous and elastic cellular polymer matrix. Figures S5 and S6 present the injected eutectic gallium-indium (EGaIn) liquid metal alloy within an elastic silicon hollow microfiber with a diameter of approximately 0.5 mm. The liquid fiber metal is flexible and stretchable as demonstrated in fig. S7 and movie S2, which endeavors the keyboard with flexibility, stretchability, and deformability. When putting all the components together, Fig. 1E demonstrates the schematic of how they are positioned. Due to the consistent intensity of the magnetic fields when penetrating through water, the keyboard is completely waterproof, ensuring stable output signals even during extreme water interactions, such as when in contact with perspiring human hands (fig. S8) (*34*).

To optimize the typing–to–electrical energy conversion of the intelligent keyboard, we systematically examined the assembly and properties of the two major components that contribute to the self-powered diagnosis working principle. To begin with, we verified the soft magnetoelastic composite. To optimize the mechanical, magnetic, and magnetoelastic properties of each key sensor unit, we investigated the different weight concentrations of the MC layer. Under continuously applied pressure, 83 wt % was deemed to be the most optimal concentration due to the highest value of magnetic field variation of 10.1 mT compared to those with 50 wt % (6.7 mT) and 33 wt % (0.9 mT) of micromagnets, as seen in Fig. 1F. The 83 wt % of the MC layer provided a strain up to 140% (Fig. 1G) and Young's modulus of 563 kPa. Further increase in concentration would hinder the proper mixing of magnetic nanoparticles and the polymer, resulting in a more rigid and less flexible product than desired. With a scalable and easy fabrication method, the intelligent keyboard offers excellent advantages in cost-effectiveness and versatile adaptability toward practical applications, working in a self-powered and self-driven manner for continuous and timely PD diagnosis.

Sensing performance characterization

The intelligent keyboard works on the basis of a coupling effect of the magnetoelastic effect in the MC layer and the MI in the MI layer. To optimize its typing sensing performance, we investigated the performance of the MC and the MI components as a single sensor unit. Each sensor has a dimension of 16 mm by 16 mm by 1 mm. To begin with, taking into consideration a user's keystroke dynamics and the mechanism of the device, when a finger presses a sensory key during the compressed state, two-level interactions occur. First, at the microscale level, the deformed shape during the compressed state causes magnetic particle–particle interaction, leading to changes in distance and variations of the particles. At the atomic scale level, magnetic dipole–dipole interactions occur, causing the rotation and movement of the magnetic dipole within the particle. Hence, the surface magnetic flux density would decrease, as seen in Fig. 2A. In addition, Fig. 2B shows that the demagnetizing fields are proportional to the decrease in the surface magnetic flux density at 3-N uniaxial pressure. Once the finger was released, the key sensor unit no longer experienced uniaxial stress. Consequently, the micromagnet wavy chain recovered to its original condition, allowing the magnetic flux density to reverse back to the initial intensity. After being compressed, the magnetic hysteresis loop of the system exhibited a decrease in both the remnant magnetization and coercive field due

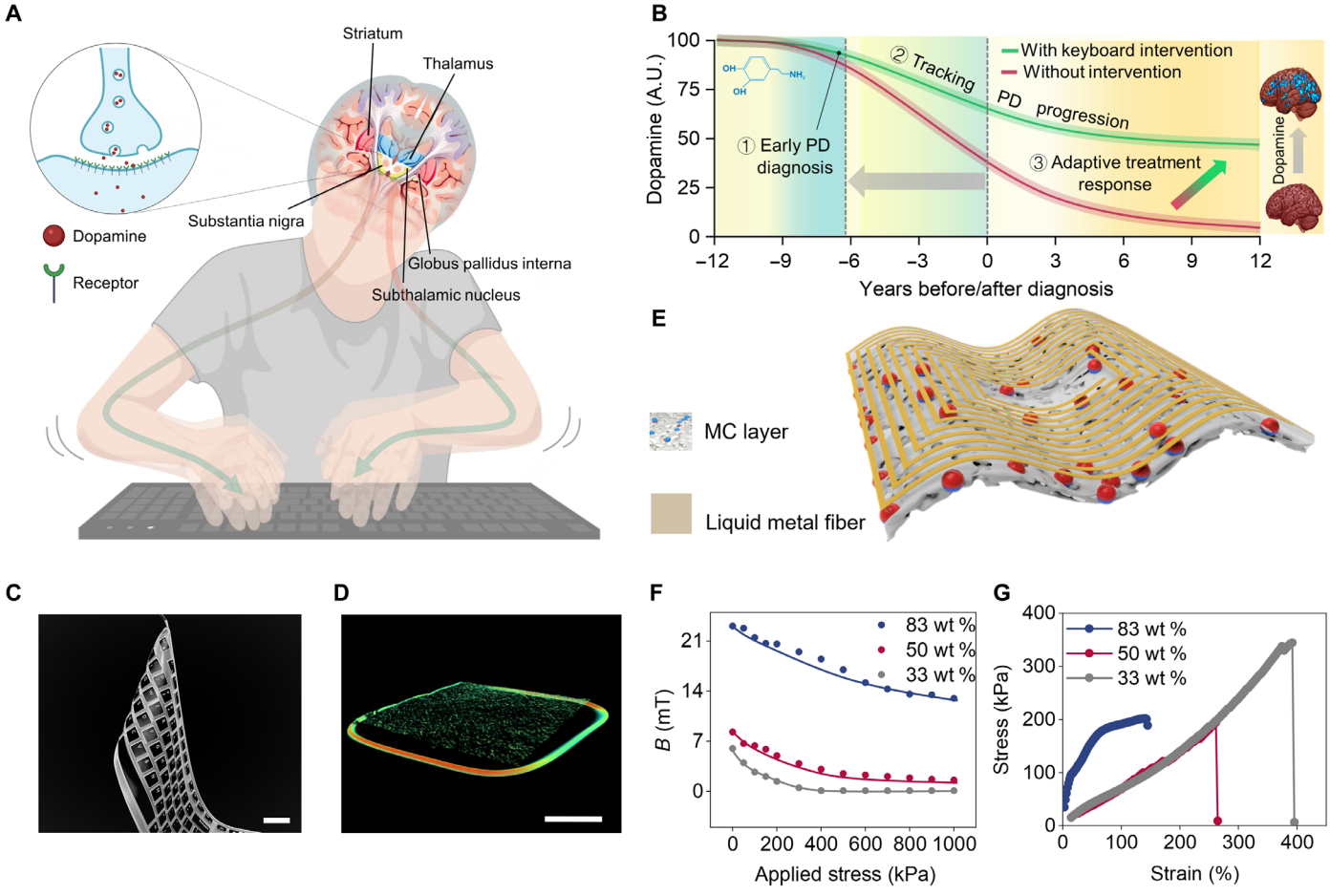

Fig. 1. A self-powered magnetoelastic intelligent keyboard to diagnose PD. (**A**) Schematic of the proposed intelligent keyboard as a conceptual diagnostic tool for patients with PD. (**B**) Graphical illustration of neurogenerative changes with and without adaptive treatment response. A.U., arbitrary unit. (**C**) Photograph showing the flexibility of the intelligent keyboard. Scale bar, 3 cm. (**D**) 3D micro-CT of a single magnetoelastic key. Scale bar, 5 mm. (**E**) Schematic design of the intelligent keyboard showing the functional layers. (**F**) Magnetic flux variations under applied compressive stress of different micromagnetic concentrations. (**G**) Stress-strain curves of the soft magnetoelastic film under different micromagnetic concentrations.

to the rearrangement of the micromagnets (fig. S9). As illustrated in fig. S10, *b* and *h* represent the horizontal and vertical distances, respectively, between the adjacent magnetic dipoles in a wavy chain.

Both the voltage and current outputs of the key sensor unit were verified with different numbers of turns. Figure 2C displays a positive relationship that agrees with Faraday's law of induction, stating that the electrical outputs are directly proportional to the number of conductive fiber turns and the magnetic field variation of the MC layer. Similarly, Fig. 2D exhibits a predictable positive linear progression between the output performance and the thickness of the device. However, because the proposed keyboard cover must maintain a slim profile to fit onto a computer keyboard, one turn of liquid metal fiber and a thickness of 1.0 mm were used to provide adequate output performance without undermining the typing comfortability for the end users. According to the National Institute for Occupational Safety and Health (NIOSH), the configuration of keyboard surfaces, including thickness and materials, has a minimal impact on user comfort as long as ergonomic typing principles are followed. These principles include maintaining a neutral posture for hands and wrists to reduce musculoskeletal problems. NIOSH also emphasized that changing a single workplace element, such as the keyboard, is unlikely to cause discomfort when proper ergonomic setups are in place. As the keyboard cover adds only 1-mm thickness and assumably no other workstation elements are altered, the impact on comfort is expected to be minimal. Instead, users should focus on several important factors such as the workstation and chair adjustability, equipment placement, and optimal lighting to ensure overall comfort and reduce strain (*35*).

In addition, to verify the response of the key sensor unit in different frequencies, we investigated the pulse waveforms subjected to 1 to 10 Hz at a fixed pressure, as illustrated in fig. S11, and observed that increasing the applied frequencies yielded higher electrical outputs. With an increased frequency, the output signals from 0.5 to 10 Hz exhibited a higher SNR up to 34.5 dB (Fig. 2E) and a shorter response time as low as 4 ms (Fig. 2F), as the MC layer became more responsive to deformation. Note S1 further clarifies the trends of the response time and SNR and the comparative data from other existing frequency-based PD diagnosing technologies. In addition, to study the sensitivity of the magnetoelastic key sensor unit, loading-unloading experiments were conducted at 1 Hz with varying applied pressure.

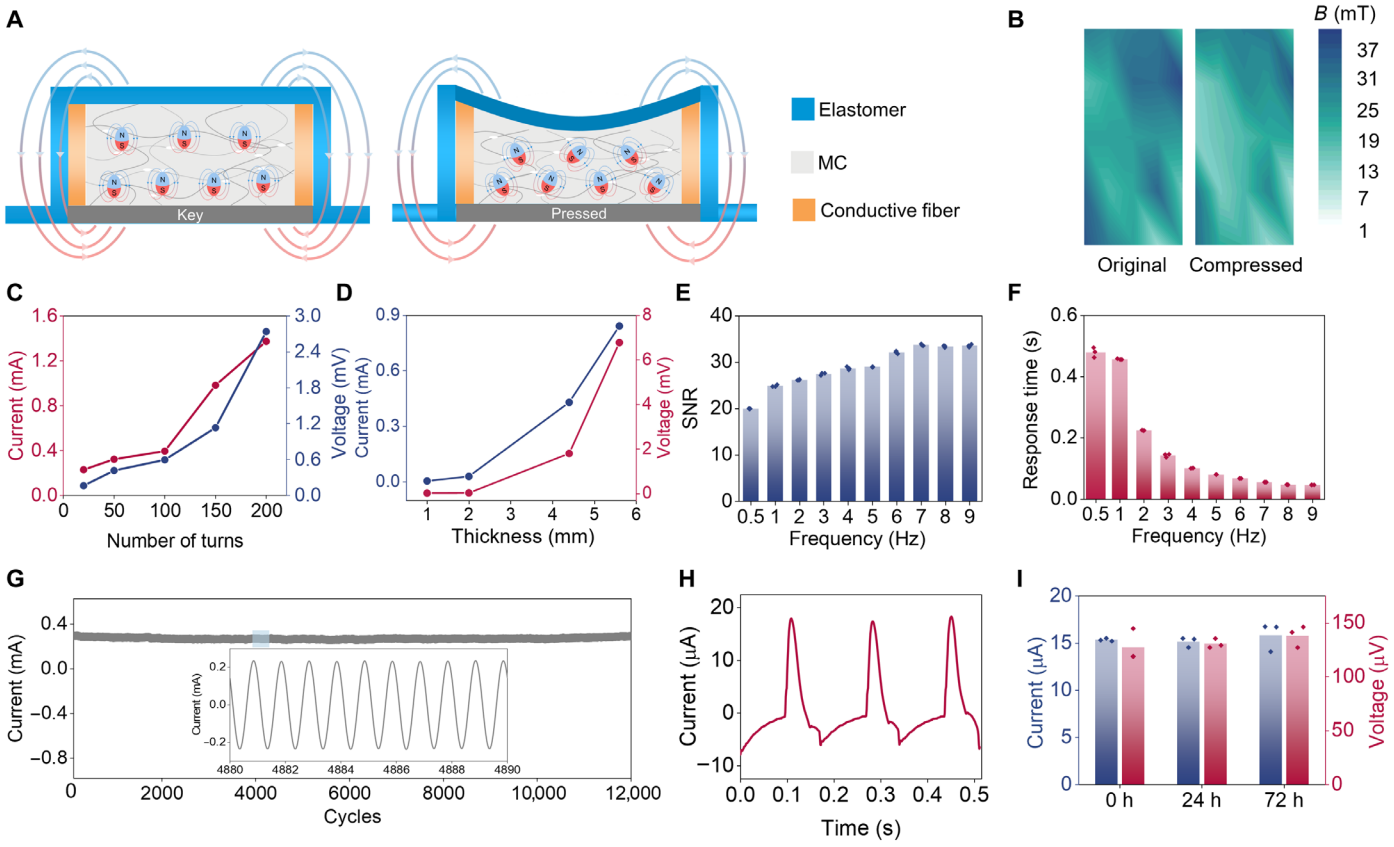

Fig. 2. Understanding the pressure sensing performance during typing. (**A**) Mechanism of the self-powered personalized keyboard. (**B**) Magnetic flux density mappings of the soft magnetoelastic film in the original state and under 3-N compression. (**C**) Dependence of current and voltage output of the magnetoelastic key on the number of turns of liquid metal fibers. (**D**) Dependence of the current and voltage output of the magnetoelastic key on the thickness of the magnetoelastic key. (**E** and **F**) Dependence of the SNR (E) and response time (F) of the magnetoelastic key, measured using current output, on a range of applied pressure frequencies. (**G**) Cyclic test of the magnetoelastic key for more than 12,000 cycles and an enlarged view of the marked region, showing excellent durability and repeatability. (**H**) Current output of finger tapping on a single key. (**I**) Stability of the keyboard after submerging in artificial sweat for 0, 24, and 72 hours.

As shown in fig. S12, the key sensor unit could detect pressure as low as 0.25 kPa. Figure 2G substantiates the durability of the sensor. With 12,000 cycles of applied uniaxial compression, the device still exhibited constant current output, exclaiming its excellent durability and repeatability. To demonstrate the robustness of the device, we conducted finger tapping on a single key and collected current and voltage signals, showing repeated data (Fig. 2H and fig. S13, respectively). The stability of the device was further evaluated under various conditions, including exposure to artificial sweat and different temperature and humidity levels. The device was submerged in laboratory-prepared artificial sweat for 24 and 72 hours. The results in Fig. 2I showed that its signals remained like the original condition even under the interference of the liquid environment. Similarly, several tests conducted at different temperature and humidity environments (fig. S14) also displayed consistent output signals, signifying the stability of the device. Last but not least, ensuring uniformity across the keyboard is critical to confirm that output signals are solely influenced by typing and not by internal variability among individual keys. To assess this, we conducted a uniformity test to measure the current signals across all 26 letters under constant force (fig. S15). Then, a one-way analysis of variance (ANOVA) revealed no significant differences between the keys, as the *P* value exceeded 0.05. This result confirmed the uniformity across the keyboard, establishing its consistency before testing with human participants.

Intelligent keyboard for behavioral biometrics of keystroke dynamics

With the fundamental working principle, together with machine learning algorithms and a cellphone APP, the IKS is a promising technology, as an application for PD progression monitoring, due to its advantages in excellent material properties that supply the end product with flexibility, stretchability, deformability, water resistance, and signal-to-function and biomechanical-to-electrical platform (Fig. 3A).

In the realm of data science, machine learning has emerged as a powerful tool for extracting personalized healthcare information from imperceptibly abnormal signals. Building upon this foundation, first, we established a laboratory-scale algorithm to differentiate three healthy users' keystroke dynamic signals. Laboratory-scale typing datasets were collected by our intelligent keyboard for the machine learning model training. Specifically, three healthy participants (a 21-year-old male, a 25-year-old female, and a 29-year-old female) were instructed to type a randomly generated English paragraph for 1 min, repeated seven times. Figure 3B and fig. S16 show

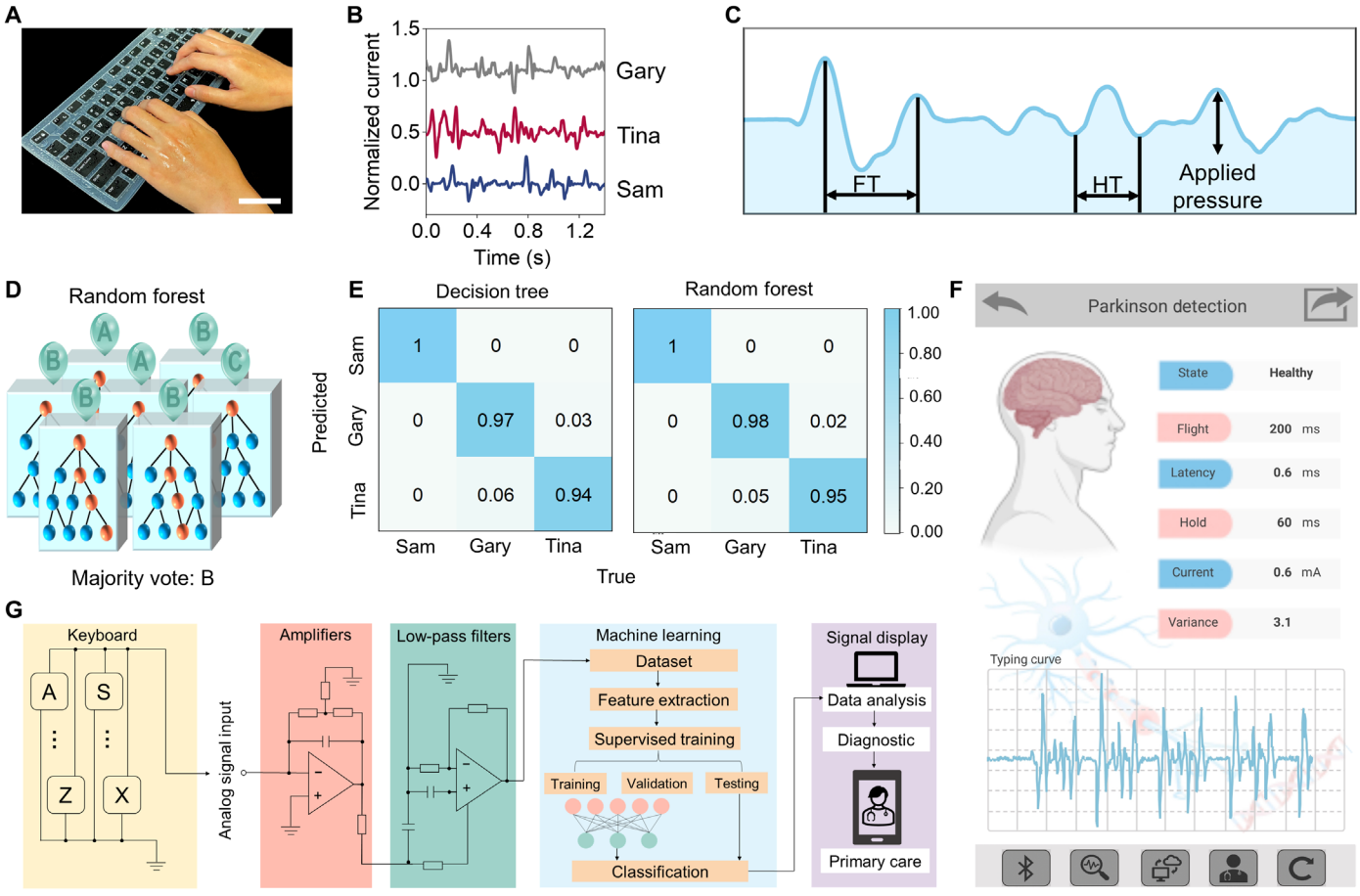

Fig. 3. Machine learning–assisted intelligent keyboard for behavioral biometrics of keystroke dynamics. (**A**) Demonstration of the intelligent keyboard with sweat-proof capability. Scale bar, 3.5 cm. (**B**) Current output of three different participants typing with the keyboard. (**C**) Features that can be detected from a waveform of typing. (**D**) Schematic RF algorithm made up of several DT algorithms. (**E**) Confusion matrices for DT and RF algorithms with efficient features to detect each healthy person typing random words. (**F**) Customized cellphone APP interface to display the typing results in the front end. (**G**) System process flow including the IKS with magnetoelastic key sensor array of the intelligent keyboard connected in parallel, an amplifying circuit, a low-pass filter circuit, a microcontroller with a machine learning algorithm, an on-board Bluetooth module, and a laboratory-developed smartphone APP or computer interface that can display and send data to physicians in one touch.

an excerpt of the signals generated by these three volunteers during typing. These generated signals containing useful information such as FT, HT, and applied pressure (Fig. 3C) were extracted and analyzed. FT is defined as the time between two peak voltages, which is the interval between releasing one key and pressing the next key. HT is the time measured within one peak, for which a key is pressed and held down before being released. Pressure is the amplitude of the current peak at which a force is applied to press the key.

In addition, these sensing signals were preprocessed by sampling a 1-s time series, generating the training records. Two sets of features were extracted from these data. The minimal features describe the data with the minimum number of features, and efficient features contain a larger number of features to describe the data. The feature type was divided into all and selected/filtered. In table S1, the number of features for each set is listed, and, meanwhile, using 10-fold cross-validation for model training, the results are also summarized. The next step after feature exaction was to keep only the relevant features. Filtering features to keep only the relevant features can reduce the computation time for both algorithms without compromising the accuracy of the model. Two classifiers—decision tree (DT) and random forest (RF)—were established to train the model. Several DTs make up an RF (Fig. 3D) (*36*). To test the capability of the model, we randomly divided the data into a test-to-training ratio of 10 to 90%. The performance of the model on the test set was reported by standard metrics of precision, recall, and F score, and the results are summarized in table S2. According to the listed results, RF with efficient features gave the most accurate result of 98.38%, as the cross-validation means accuracy. The confusion matrices in Fig. 3E compare the performance of the classifiers on the test set. The AUC represents the average of the one-on-one area under the curve values calculated for different pairs of classes. Ultimately, RF outperformed DT for all regimes of the test set.

Cellphone APP for the IKS

We also developed the intelligent keyboard into an IKS with a wireless, Bluetooth platform technology, including a keyboard cover, a microcontroller with machine learning algorithms, and a prototype of a customized cellphone APP for data display, storage, and sharing (Fig. 3F). The typing signals generated by the intelligent keyboard were first passed through a data acquisition–transmission system to

ensure high-quality signal conditioning. Specifically, these signals were processed through the signal preprocessing unit (fig. S17A), starting with a preamplifier (AD8429), which provides high-gain amplification of low-level signals while maintaining low noise performance. The amplified signals were subsequently filtered using a band-pass filter (AD828) to remove unwanted frequency components and isolate the relevant signal range, ensuring a clean and noise-free signal for further stages. Last, a post-amplifier (AD603) boosted the signal strength to a level suitable for accurate processing by downstream components. The processed signals were fed into a microcontroller (Arduino Nano RP2040 Connect) (fig. S17B), which digitizes the analog data using its integrated analog-to-digital converter and processes them using machine learning algorithms. The algorithm distinguishes and expectedly provides an estimated assessment of PD subtypes based on the calculated values of FT, latency, HT, current, and variance. The processed signals were then wirelessly transmitted to a Bluetooth low energy–enabled cellphone, which serves as the central interface for real-time display and sharing. The system process chart for the IKS is represented in Fig. 3G. Figure S18 and movie S3 demonstrate the real-time delivery of typing signals from a perspiring hand to the cellphone APP. Figure S19 showcases the screenshots of the APP's interface, and movie S4 reflects its ability to wirelessly receive, store, and transmit data to third-party recipients via different types of sending APPs such as email and message. All these patient-generated data can be one-click forwarded to physicians for PD diagnosis through email, cloud electronic health records, or messages for further feedback. Briefly, the machine learning–assisted IKS serves as a quantitative tool for monitoring the progression of PD and provides physicians with numerical data for standard notifications and warnings of the patient's health status.

Evaluation of the IKS for PD diagnosis in a clinical setting using deep learning

To further examine the system toward real-life applications, we conducted a pilot human study with PD patients at the University of California, Los Angeles (UCLA) Neurology Clinic (approved institutional review board no. 21-000974). Three patients with PD were recruited and assigned a unique identification number. On the basis of visual observation, patient 3 appeared to have more severe symptoms due to their slow gait and sporadic movements. Figure S20 displays the experimental setup, while Fig. 4A and movie S5 showcase the hands of a patient with PD on the intelligent keyboard, typing random English words for 1 min, repeated three times, and performing a reaction time (RT) experiment, repeated five times. In an earlier approach to classifying between three different healthy participants, features from the time-series signals generated by the intelligent keyboard, such as statistical measures, frequency-domain characteristics, and time-domain peaks, were manually extracted and selected. However, as the dataset size increased, the classification accuracy of these shallow models—DT and RF—markedly declined.

To address these limitations, we implemented a deep-learning framework based on a convolutional neural network (CNN). Rather than manually selecting features for the model, the entire time-series signals—encompassing all typing-relevant biomarkers such as intentional keystroke events, tremor-induced noise, and FT—were fed directly into the CNN. This end-to-end strategy enables the network to automatically learn the most discriminative features for distinguishing PD typing signals from those of healthy participants. Consequently, explicit feature engineering or filtering of tremor-induced noise is unnecessary, as the convolutional layers inherently act as automatic feature extractors, focusing on the most relevant patterns for classification. Unlike DT and RF, which rely on human-defined features, CNN operates on a more abstract representation derived from the entire signal.

The deep-learning pipeline includes (i) data collection and augmentation, (ii) CNN model training, validation, and testing, and (iii) investigating how the CNN automatically extracted relevant features during the training process, highlighting its ability to serve as an automatic feature extractor that focuses on the most pertinent patterns for PD classification. Figure 4B summarizes the deep-learning framework used in our data analysis method.

In data collection and augmentation, a total of 16 individuals participated in the human study, including three patients diagnosed with PD. Each participant was instructed to perform similar typing tasks using the intelligent keyboard, which was used to collect time-series electrical signals. The collected time-series signals were segmented into fixed slices, with each slice containing 20,000 data points.

Given the smaller number of patients with PD (3 people) compared to healthy participants (13 people), the CNN classifier risked learning to achieve high accuracy by predominantly classifying all signals as belonging to healthy participants. To mitigate this bias, we augmented the intelligent keyboard–generated time-series electrical signals from patients with PD using the following techniques to balance the sample sizes between the two categories. Temporal inversion reversed the sequence of the intelligent keyboard–generated time-series electrical signals, simulating alternative dynamic responses by altering their temporal order. Amplitude inversion vertically inverted the intelligent keyboard–generated time-series electrical signal amplitude, introducing variability in the waveform's representation and analysis. Temporal-spatial inversion combined temporal and amplitude inversions to create comprehensive alterations in intelligent keyboard–generated time-series electrical signal characteristics, further diversifying the dataset. Permutation segmented the original intelligent keyboard–generated time-series electrical signals into smaller parts, which were then randomly rearranged, challenging the model to maintain accuracy despite disruptions in chronological sequence. Last but not least, time warping selectively elongated certain intelligent keyboard–generated time-series electrical signal segments, introducing variations in temporal dynamics to simulate different scenarios.

Following augmentation, we obtained 164 samples for the healthy subject category (HES) and 175 samples for the PD patient category (PDP). In addition to balancing the sample sizes between the two categories, these augmentation techniques enhanced the variety of the training data without requiring additional data collection. By introducing variability into the dataset, these data augmentation methods prevented the model from memorizing specific features, thereby reducing the risk of overfitting—an established practice in the computer science community (*37*–*39*).

The second step of the deep-learning pipeline is CNN model training, validation, and testing. Developing a deep-learning model entirely from the ground up is often challenging due to the considerable computational resources and extensive training data it demands. To address these challenges, we adopted transfer learning, a technique widely recognized to adapt pretrained neural networks to different tasks (*40*–*42*). For our study, we used a pretrained CNN initially developed to classify images across 1000 categories (*43*). This network, trained on a large and varied dataset, is known for its

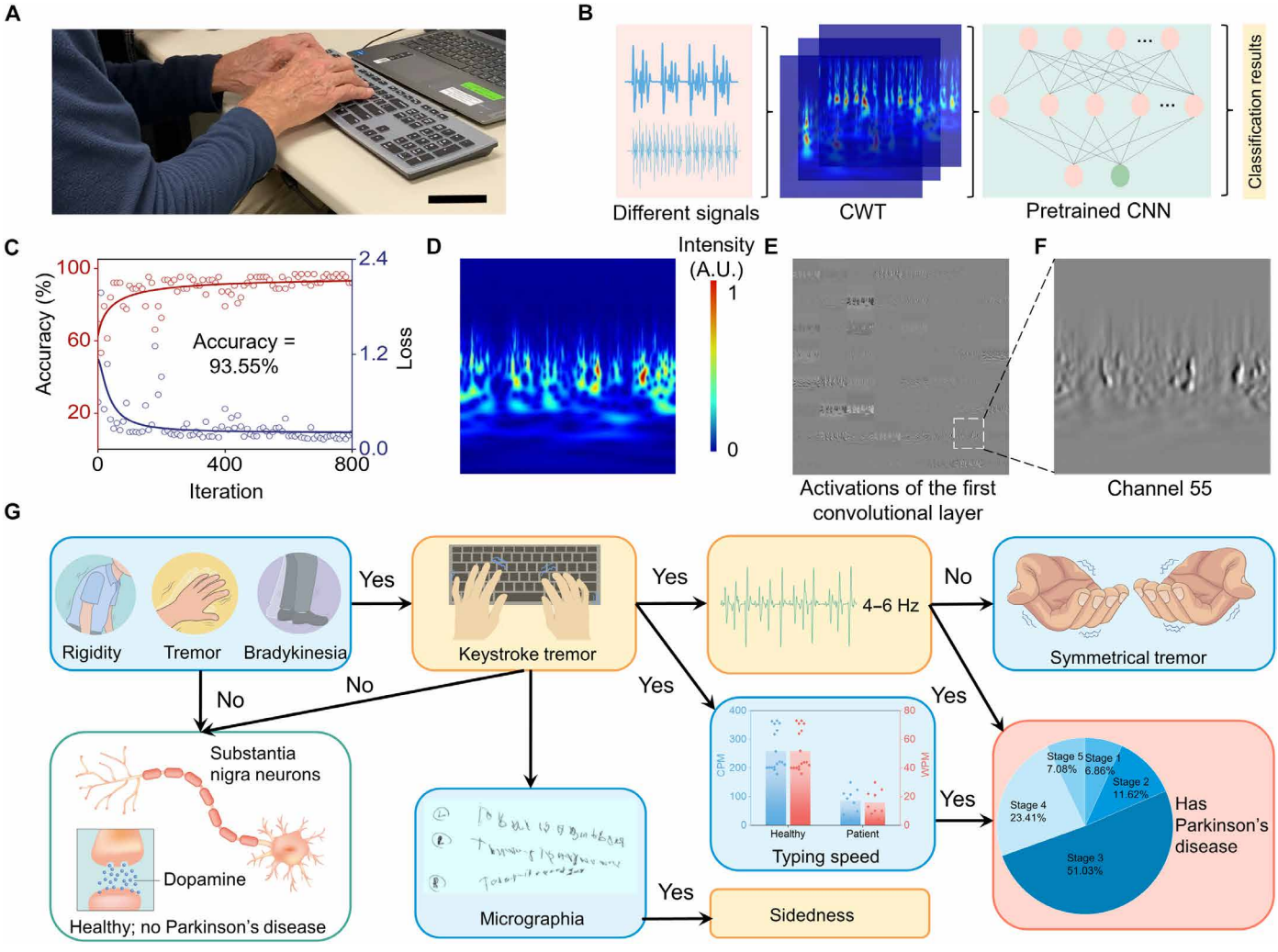

Fig. 4. The IKS for diagnosing PD using deep learning. (**A**) Photograph of patients with PD typing on IKS. Scale bar, 6 cm. (**B**) Presentation of the CNN framework. (**C**) Training process of the CNN, including the validation accuracy and the loss function evolved in relation to the number of iterations. (**D**) Time-frequency representation image generated from a slice of original signals from the PD patient typing. (**E**) Output activations of the first convolutional layer in an 8-by-8 grid, one for each channel in the layer. (**F**) Channel 55 exhibits the highest activation. (**G**) Predictive model from the generated data. This flowchart is for illustrative purposes only and does not represent actual clinical or machine learning correctness.

strong performance in image recognition tasks. By leveraging this robust foundation, we tailored the network to analyze intelligent keyboard–generated time-series electrical signals. This approach elegantly sidestepped the challenges posed by limited data, allowing us to achieve robust performance without needing to start from scratch.

To convert the intelligent keyboard–generated time-series electrical signals into images suitable for classification by the pretrained CNN model (fig. S21A), we used the continuous wavelet transform (CWT) to generate time-frequency representations, known as scalograms (fig. S21B), in the MATLAB Wavelet Toolbox. A scalogram captures the absolute value of the CWT coefficients of a signal, offering a detailed visualization of its frequency content over time. These time-frequency representations effectively preserved key typing-related information, such as short, sharp signal changes from keystroke events and distinct frequency oscillations associated with tremors. This transformation not only retained the essential typing signal characteristics but also rendered them interpretable by CNN, enabling the model to autonomously determine which features are most indicative of PD versus healthy typing patterns.

After conversion, 10% of the samples were reserved as an unseen test set, while the remaining samples were split into 80% for training and 20% for validation. The labels (HES or PDP) of these samples served as the ground truth for supervised learning. Specific modifications were made to adapt the model to our task, such as replacing the fully connected layer with a configuration that outputs the number of classes (two: HES and PDP). The convolutional layers extract time-frequency representation features, while the dropout layers help prevent overfitting by randomly deactivating a portion of neurons during training (*44*). The training process was carried out using the MATLAB Parallel Computing Toolbox and Deep Learning Toolbox. After approximately 800 iterations (Fig. 4C), the tuned CNN model achieved a classification accuracy of 93.55% on the validation set (fig. S22A) and 96.97% on the test set (fig. S22B). Detailed performance metrics, including the

confusion matrix, precision, recall, and F1 score, are provided to support the evaluation (Table 1).

The third step of the deep-learning pipeline is to investigate how CNN automatically extracted relevant features during training. The results confirmed that by leveraging a pre-trained CNN model and transfer learning techniques, the fine-tuned CNN could autonomously learn features from the time-frequency representations of the intelligent keyboard–generated time-series electrical signals—thereby classifying them as HES or PDP.

Convolutional layers in the network act as filters that extract distinct image features. Early layers typically learn common features such as edges, blobs, and color variations on the time-frequency representations. To demonstrate this process, we analyzed the network activations and compared regions of high activation with the original time-frequency representations. For instance, we displayed an original scalogram image (Fig. 4D), which is a time-frequency representation of the intelligent keyboard–generated time-series electrical signals, alongside the activations of the first convolutional layer (Fig. 4E).

A CNN layer contains multiple two-dimensional (2D) grids, known as channels. Each section of the activation map represents the response of a channel in the first convolutional layer. Bright areas indicate a strong positive response. Dark areas indicate a strong negative response. Gray areas show little to no reaction to the input. We found that channel 55 exhibited the highest activation (Fig. 4F). By comparing this channel with the original time-frequency representations, we saw that it activated on the bright color regions (indicative of frequency differences), implying that the first convolutional layer primarily learns features related to the frequency variations in the signals.

While end-to-end deep learning may appear to function as a "black box," understanding exactly how features are extracted could be an active area of research in the computer science community (*45*). This ongoing theoretical investigation lies beyond the scope of our current work, which focused on developing an intelligent keyboard and demonstrating a proof-of-concept approach for classifying signals using deep learning.

To further examine PD motor symptoms, fig. S23A shows a 3-s data excerpt of each patient's normalized typing pattern, and fig. S23 (B to D) shows a 20-s excerpt. Movie S6 shows real-time generated data displayed on a computer. Besides the typing patterns, we also collected the participants' characters per minute (CPM), words per minute (WPM) (fig. S24), FT, HT, and RT (fig. S25) data for additional comparison with healthy participants. Using the Mann-Whitney *U* test, statistical differences ($P < 0.05$) were noted between patients with PD and healthy participants in these metrics. The Mann-Whitney *U* test was chosen because of its nonparametric nature. Because typing performance often varies on the basis of motor skills and impairments, the data distribution might not be normal. Movie S7 demonstrates how the patients' RT was examined. Upon observation, patients with slower and more rigid keystroke dynamics or higher severity would exhibit more minor peaks. In particular, patient 3, who demonstrated more difficulties in their physical movements compared to others with more fluent typing movements, produced more minor peaks and data gaps. Observably, while pressing each key and moving to the next key, patient 3 produced many tremor noises. Conversely, the correlation occurred with patient 2, whose CPM and WPM data were highest, and who also expectedly displayed the highest fluency in the observed electrical signals.

In conclusion, the pilot study demonstrated the feasibility of the intelligent keyboard in converting keystroke dynamics to high-fidelity electrical signals even with subtle changes. Typical PD biomarkers such as slow movement, RT, and tremors could be quantitatively indicated via the collected data, showing timing and pressure-related information. In addition, the patient's severity, as measured by the MDS-UPDRS, was unknown, as it was only assessed at the initial examination by physicians. We also relied on visual observation to assess the relationship between PD patient severity and keystroke dynamics. Comparing the dataset with the gold standard MDS-UPDRS assessed at the time of the experiment would provide a more accurate evaluation of the intelligent keyboard's performance. Figure 4G illustrates a hypothetical flowchart that integrates various features to facilitate a comprehensive evaluation of PD progression. The IKS provides valuable insights and lays the foundation for further advancements in personalized medicine, particularly in the context of PD therapeutics and medication titration.

IKS' technical advancements

In comparison to previously published research on keystroke dynamics for monitoring the progression of PD, our research has focused on designing a fundamentally innovative platform technology. While several previous works have targeted at-home tracking of PD progression through keystrokes, our work has introduced the following advancements that were not addressed before.

From a fundamental principle point of view, our IKS leverages the giant magnetoelastic effect. The magnetoelastic effect—the variation of a material's magnetic field under mechanical stress—is usually observed in rigid metal alloys such as $Tb_xDy_{1-x}Fe_2$ (Terfenol-D) and Ga_xFe_{1-x} (Galfenol), under an externally applied magnetic field. This limitation in rigid metal alloys makes them limited to the use in building vibration control (*46*). In 2021, our research group discovered

Table 1. Evaluation metrics.

	Precision	Recall	F1 score
Validation set			
HES	0.9333	0.9333	0.9333
PDP	0.9375	0.9375	0.9375
Testing set			
HES	0.9412	1	0.9697
PDP	1	0.9412	0.9697

the giant magnetoelastic effect in soft material systems, paving the way for the development of soft bioelectronics (*34*). This work marks the first instance of leveraging the giant magnetoelastic effect in soft systems for keystroke dynamics analysis, promoting a cutting-edge paradigm to the PD research community. This innovation endows our keyboard with several advantages including self-powered sensing, waterproofness, biocompatibility, scalable fabrication, portability, and durability. The self-powered nature of the keyboard enables wireless and continuous monitoring of typing motions, converting both the keystroke pressure and timing data into high-fidelity electrical signals.

From a technological advancement point of view, the IKS emerges as a transformative breakthrough in personalized keystroke analysis for PD progression. Its ability to quantitatively capture intricate biometric signals surpasses conventional keyboard tools used for PD assessment. The electrical signals generated by the IKS are directly correlated with key presses, providing comprehensive information on the typing pressure, RT, FT, and HT during keyboard usage. The results display timestamps for the press and release events of every keystroke. While recent works have analyzed keystroke dynamics, these efforts are often constrained by the limitations of traditional store-bought hardware, which generally lacks integrated sensor systems. For example, research works that focus on a keyboard for PD progression have used standard, wired commercial keyboards (*26*, *29*–*32*), which fall short in terms of innovative hardware design. The omission of pressure data when using a conventional keyboard substantially limits the depth of analysis. Our work, in contrast, addresses this gap by introducing an innovative keyboard technology that fundamentally enhances real-time data capture at the hardware level.

Another point relevant to the technological advancements of the IKS is its ability to capture not only temporal data but also pressure metrics during typing. This feature distinguishes it from traditional keyboards, allowing for a more detailed analysis of motor symptoms exhibited during typing, which is relevant to PD (*9*). By integrating both pressure and temporal information, our technology mitigates the potential biases of merely time-domain analysis alone, offering a more symptom-oriented evaluation. This approach not only enhances diagnostic specificity but also sheds light on the detailed motor symptomatology associated with PD, surpassing the capabilities of conventional typing assessments.

From a translation point of view, the IKS has demonstrated considerable potential in a clinical setting. The system provides real-time data on keystroke dynamics, which allows us to assess motor function in a noninvasive manner. Our design seamlessly integrates into the daily lives of patients with minimal burden. Furthermore, the design is centered on scalability, cost-effectiveness (table S3), and user-friendliness, enabling mass production and widespread deployment across various healthcare settings and at home. The self-powered nature reduces reliance on external power sources, and its wireless capability facilitates its integration into telemedicine and at-home testing frameworks. In addition, the biocompatible materials and durable construction ensure that the IKS can be used consistently and continuously over extended periods without causing discomfort or requiring frequent maintenance. This study provides preliminary evidence that our IKS can serve as a complementary method for personalized monitoring of PD progression. Our IKS captures richer PD-relevant data, encompassing patients' typing pressure, RT, FT, and HT, than commercial keyboards, achieving high accuracy.

From a practical impact point of view, the IKS offers a tangible solution to the quality of life for patients with PD. It provides continuous, real-time monitoring of motor symptoms to facilitate patients and clinicians with actionable data that can influence treatment decisions. The practicality of the IKS extends beyond its diagnostic capabilities, supporting everyday communication and improving portability and ease of transport for use in various environments. By combining these features, the IKS addresses medical needs and enhances user experience. In contrast, other works have not emphasized the advancement of keyboard technology, often relying on traditional, wired, and standard keyboards. For instance, the Quantitative DigitoGraphy (*25*, *28*), one of the few custom-built devices, requires a bulky, wired setup and external power supply, complicating its practical use in everyday life. Our keyboard, however, is designed to be waterproof, portable, wireless, and flexible. Thus, the IKS not only redefines the technological landscape of personalized PD monitoring but also enhances the daily usability and overall patient experience. Here, we present table S4, which compares existing studies where a physical keyboard was provided to patients for monitoring PD progression. We excluded papers that focus solely on predictive algorithms or smartphone software, as they would be less relevant compared to our primary physical platform technology.

In conclusion, the IKS is a specialized, self-powered keyboard designed from the ground up to offer a comprehensive solution. It integrates advanced sensing hardware and leverages the giant magnetoelastic effect, enabling real-time data capture, scalability, and patient-centered features. The IKS empowers patients and healthcare professionals with actionable insights into PD progression.

DISCUSSION

In this work, we explored the use of the quantitative measures obtained from the intelligent keyboard to assess PD symptoms. The intelligent keyboard is capable of converting keystroke dynamics into electrical outputs, implementing the signal-to-function principle in monitoring the symptoms of PD. This, in turn, enables personalized drug titration and helps prevent underdoing and overdosing. Hence, the intelligent keyboard can detect signals in different frequencies relating to PD tremors (4 to 6 Hz) and within human motions (0.5 to 10 Hz), maintain a stable electrical output with perspiring hands, and exhibit an appropriate limit of detection as low as 0.25 kPa, a short response time of 4 ms, an SNR of 34.5 dB, and durability after 12,000 testing cycles. In addition, it exhibits flexibility, stretchability, and waterproofness. Assisted with machine learning algorithms, the intelligent keyboard could distinguish different user's keystroke dynamics with an average prediction accuracy of 96.67%. As proof of concept, the intelligent keyboard was combined with the cellphone APP to become an IKS, which could deliver typing data wirelessly and, through machine learning algorithms, characterize the generated data into PD-related parameters.

Furthermore, we conducted a pilot human study using the IKS to analyze keystroke patterns of patients diagnosed with PD. The IKS successfully converted their typing movements into readable electrical signals with distinct alterations in keystroke dynamics such as prolonged typing time, extended pauses, and diminishing hand motor skills. These alterations were quantitatively captured in the generated waveforms. Typing style also varied across participants such as text typed and the speed of the typist. The problem of typing heterogeneity was addressed by three approaches, including the

measurement of HT, local typing windows, and automatic data learning patterns. Key presses and releases were largely unaffected by the text being typed, typing speed, or individual typing habits. In the first approach, we looked at HT, which is not under one's conscious control. Hence, previous studies concluded that HT provides information on bradykinesia effects that prevent patients with PD from lifting their fingers from keys in a consistent pattern (*22*, *26*). Second, we focused on the characteristics of typing in a short period between each key to help capture subtle variations in motor performance. Last, machine learning algorithms also compared typing patterns between the patients with PD and a control group. The information from the three approaches allows us to establish a personalized baseline, where individuals with variations in typing skills can be monitored for motor function changes over time, aligning with PD's progressive nature.

While this study provides promising results, it is important to acknowledge its limitations as a preliminary investigation. First, the validation of the system was performed with a small sample size of the patient cohort in a controlled setting. A larger and more diverse patient cohort would offer a more comprehensive and robust assessment of the device's reliability and applicability. Second, the current study focused on short-term typing tasks. Thus, it lays the groundwork for future longitudinal studies aimed at monitoring PD over a long-term, continuous manner, to evaluate the device's utility in capturing the disease's inherently slow progression over months and years. This would provide clinicians with more comprehensive datasets to monitor PD's progression. Last, while the initial system successfully captured specific quantitative data, translating these findings into functional clinical outcomes, such as predicting optimal medication regimes, requires further validation through longitudinal studies and clinical trials.

In the future, the IKS could also be integrated into therapeutic interventions, enhancing its utility in clinical settings. Because typing on a keyboard requires complex coordination among visual and procedural memory, language, and motor function, the IKS could serve as a real-time evaluation for typing metrics during ON and OFF states. By correlating with changes in keystroke parameters, clinicians could tailor the timing and dosage of dopaminergic medications. In the context of deep brain stimulation (DBS), by monitoring typing behaviors before, during, and after DBS interventions, the IKS could provide valuable insights into the effects or potential side effects of DBS therapy on a patient's motor performance or dystypia. These data could assist in fine-tuning DBS parameters to achieve optimal therapeutic outcomes for individual patients. The integration of IKS into therapeutic interventions offers a promising avenue for expanding its clinical application, enabling continuous and personalized assessments in both at-home and clinical settings. Future studies could benefit from exploring these individual use cases to broaden their clinical impact.

In summary, this initial study proves that the overall IKS could serve as a complementary tool, assisting clinicians with quantitative examination in an easy, at-home manner, for diagnosing PD. The combination of quantitative measures of keystroke pressure, FT, RT, and HT obtained through the intelligent keyboard, along with machine learning algorithms and a cellphone APP to create an inclusive IKS, offers a promising approach for assessing PD progression, optimizing medication regimens, and personalizing treatments. One of the noteworthy advantages of the IKS is its ubiquity as a household keyboard, coupled with its straightforward examination procedures. It can serve as an objective, quantitative, and at-home personalized biomarker for disease progression and medication response in patients with high-risk PD. The convenience of performing the test at anytime and anywhere, with results instantly one-click delivered to the desired recipient, further enhances its usability and practicality. Further research and development in this area, focusing on tracking and quantifying variations in typing features over time, allow for a more comprehensive understanding of disease progression and hold great promise for improving personalized medicine and enhancing patient care in the context of PD.

MATERIALS AND METHODS

Fabrication of the MC layer

First, the MC layer was prepared by thoroughly mixing the uncured silicone rubber matrix Ecoflex 00-30 part A and B and 65-μm nonmagnetized neodymium-iron-boron micromagnets [MQP-AA4-B+(-150m)-10215-090] with a stirring rod. The mixture was then poured into a rectangular mold for curing in a 60°C oven for 4 hours or overnight. The curing also introduced air bubbles on a micrometer scale. The weight concentrations of the micromagnets were 33, 50, and 83 wt %. The cured magnetoelastic film was magnetized by an impulse field (~2.6 T) using an impulse magnetizer (ASC Scientific, IM-10-30).

Fabrication of the MI layer

To make a liquid metal alloy, Ga (99.99%) and In (99.99%) ingots from RotoMetals were mixed to get EGaIn (74.5% Ga and 25.5 wt % In) by heating in a muffle furnace (Thermo Fisher Scientific) at 200°C for 2 hours. To increase the processibility of liquid metal and the viscosity without sacrificing its conductivity, 10 wt % Ni particles (99.5%, 5 μm; US Research Nanomaterials) were added and mixed thoroughly using a VWR Mini Vortexer. To make the liquid metal fiber, first, an elastic silicone microfiber was fabricated by thermal drawing via industrial scale level. After cutting the silicone hollow microfiber to a desired length, the liquid metal alloy was vacuumed into the elastic hollow channel. A metal conductive wire was inserted into the opening ends, fully contacted with the inner EGaIn liquid for electrical tests. Last, the opening ends were sealed by light-cured glue to avoid leakage of the inner EGaIn liquid. The liquid metal fibers were embedded into the elastomer keyboard cover using a thin-coated polymer.

Standard characterization of the MC layer

The micromagnet size distribution was imaged by SEM (ZEISS Supra 40VP). Magnetic flux density measurement was succeeded using a digital Gauss meter (TUNKIA, TD8620). The magnetic field variation was calculated by applying a linear best-fit line and taking the difference between the initial and final values. The stress-strain curves were tested at a stretching rate of 5.0 mm/s using a dynamic mechanical analyzer (Instron, 5564). Young's modulus was calculated by applying a neo-Hookean model to fit the curve.

Artificial perspiration preparation

Artificial perspiration was used to test waterproof capability. A mixture of 4.65 g of NaCl (Sigma-Aldrich), 3.87 g of 1 M lactic acid solution (Alfa Aesar), 1.80 g of urea (Alfa Aesar), 1.37 g of KCl (Sigma-Aldrich), 0.0276 g of uric acid (Alfa Aesar), 0.756 g of $NaHCO_3$ (Sigma-Aldrich), 0.546 g of 1 M $NH_3{\cdot}H_2O$ (Sigma-Aldrich), 0.175 g

of Na_2SO_4 (Sigma-Aldrich), and 1 liter of deionized water was mixed for 30 min.

Performance measurement

The voltage and current signals of the IKS were measured using a system electrometer (SR560 and SR570, respectively). A flat plate was connected to an electrodynamic shaker system, consisting of a function generator (Newark, AFG1062), a linear power amplifier (Labworks Inc., PA-151), and an electrodynamic transducer (Labworks Inc., ET-126HF) to mimic human finger tapping at a consistent voltage and frequency. The durability of the device was characterized using the electrodynamic transducer (Labworks Inc., ET-126HF).

Commercial software

CPM and WPM were collected using a commercially available software called "Typing Speed Test" developed by J. Waalboer. RT was collected using a software called "RED LIGHT - GREEN LIGHT Reaction Time Test" developed by J. Allen from the University of Washington.

Statistical analysis

Comparisons between healthy participants and patients with PD were performed using the Mann-Whitney *U* test. Comparisons between current signals from each key press were performed using the one-way ANOVA test. Python software was used for all statistical evaluations.

Data collection

For the laboratory-scale typing data collection, three healthy volunteers typed randomly generated words for 1 min and repeated the task seven times using a commercially available software called Typing Speed Test developed by J. Waalboer. Three patients with PD and other healthy volunteers each use the same software but perform 1-min typing and repeat three times.

Mobile APP design

A customized Android cellphone APP for data display, storage, and sharing was designed using MIT AI2 Companion. The typing patterns were acquired and processed with the assistance of machine learning algorithms. Then, these data were transmitted to the cellphone APP and displayed in the front end.

Human participant study

The IKS was tested using human participants in compliance with all the ethical regulations under the protocol (ID no. 21-000974) approved by the Institutional Review Board at UCLA. All participating individuals, who belong to UCLA and its Neurology clinic, were provided informed consent before participating in the study. The deep learning analysis of human participant data was conducted on an NVIDIA GTX 4070 GPU, adopting and modifying the Classify Time Series Using Wavelet Analysis and Deep Learning and Visualize Activations of a CNN function in MATLAB R2024.

Supplementary Materials

The PDF file includes:

Figs. S1 to S25
Tables S1 to S5
Note S1
Legends for movies S1 to S7
References

Other Supplementary Material for this manuscript includes the following:

Movies S1 to S7

REFERENCES AND NOTES

1. W. Yang, J. L. Hamilton, C. Kopil, J. C. Beck, C. M. Tanner, R. L. Albin, E. Ray Dorsey, N. Dahodwala, I. Cintina, P. Hogan, T. Thompson, Current and projected future economic burden of Parkinson's disease in the U.S. *NPJ Parkinsons Dis.* **6**, 15 (2020).
2. K. J. Black, H. K. Acevedo, J. M. Koller, Dopamine buffering capacity imaging: A pharmacodynamic fMRI method for staging Parkinson disease. *Front. Neurol.* **11**, 370 (2020).
3. C. D. Marsden, Problems with long-term levodopa therapy for Parkinson's disease. *Clin. Neuropharmacol.* **17**, S32–S44 (1994).
4. L. Kalilani, D. Friesen, N. Boudiaf, M. Asgharnejad, The characteristics and treatment patterns of patients with Parkinson's disease in the United States and United Kingdom: A retrospective cohort study. *PLOS ONE* **14**, e0225723 (2019).
5. A. Rankin, C. A. Cadogan, S. M. Patterson, N. Kerse, C. R. Cardwell, M. C. Bradley, C. Ryan, C. Hughes, Interventions to improve the appropriate use of polypharmacy for older people. *Cochrane Database Syst. Rev.* **2018**, CD008165 (2018).
6. L. H. Goetz, N. J. Schork, Personalized medicine: Motivation, challenges and progress. *Fertil. Steril.* **109**, 952–963 (2018).
7. C. G. Goetz, S. Fahn, P. Martinez-Martin, W. Poewe, C. Sampaio, G. T. Stebbins, M. B. Stern, B. C. Tilley, R. Dodel, B. Dubois, R. Holloway, J. Jankovic, J. Kulisevsky, A. E. Lang, A. Lees, S. Leurgans, P. A. LeWitt, D. Nyenhuis, C. W. Olanow, O. Rascol, A. Schrag, J. A. Teresi, J. J. Van Hilten, N. LaPelle, Movement Disorder Society-sponsored revision of the Unified Parkinson's Disease Rating Scale (MDS-UPDRS): Process, format, and clinimetric testing plan. *Mov. Disord.* **22**, 41–47 (2007).
8. P. Martínez-Martín, C. Rodríguez-Blázquez, M. Alvarez, T. Arakaki, V. C. Arillo, P. Chaná, W. Fernández, N. Garretto, J. C. Martínez-Castrillo, M. Rodríguez-Violante, M. Serrano-Dueñas, D. Ballesteros, J. M. Rojo-Abuin, K. R. Chaudhuri, M. Merello, Parkinson's disease severity levels and MDS-Unified Parkinson's Disease Rating Scale. *Parkinsonism Relat. Disord.* **21**, 50–54 (2015).
9. W. R. Adams, "Chapter 20—Keyboard typing for the detection of early Parkinson's disease" in *Diagnosis and Management in Parkinson's Disease*, C. R. Martin, V. R. Preedy, Eds. (Academic Press, 2020), pp. 331–344.
10. G. Alves, T. Wentzel-Larsen, D. Aarsland, J. P. Larsen, Progression of motor impairment and disability in Parkinson disease: A population-based study. *Neurology* **65**, 1436–1441 (2005).
11. J. Jankovic, Parkinson's disease: Clinical features and diagnosis. *J. Neurol. Neurosurg. Psychiatry* **79**, 368–376 (2008).
12. S. Kar, T. Aung, Impact of DaTscan in the clinical evaluation of patients with diagnostically uncertain parkinsonism. *Metric J.* **1**, 20–23 (2015).
13. K. Swarztrauber, B. G. Vickrey, Do neurologists and primary care physicians agree on the extent of specialty involvement of patients referred to neurologists? *J. Gen. Intern. Med.* **19**, 654–661 (2004).
14. K. D. Seifert, J. I. Wiener, The impact of DaTscan on the diagnosis and management of movement disorders: A retrospective study. *Am. J. Neurodegener. Dis.* **2**, 29–34 (2013).
15. D. G. Grosset, K. Tatsch, W. H. Oertel, E. Tolosa, N. Bajaj, A. Kupsch, J. T. O'Brien, J. Seibyl, Z. Walker, P. Sherwin, C. Chen, I. D. Grachev, Safety analysis of 10 clinical trials and for 13 years after first approval of ioflupane ^{123}I injection (DaTscan). *J. Nucl. Med.* **55**, 1281–1287 (2014).
16. W. C. Koller, B. Vetere-Overfield, R. Barter, Tremors in early Parkinson's disease. *Clin. Neuropharmacol.* **12**, 293–297 (1989).
17. J. S. Schneider, S. G. Diamond, C. H. Markham, Parkinson's disease: Sensory and motor problems in arms and hands. *Neurology* **37**, 951–956 (1987).
18. M. Dione, J. Wessberg, Human 8- to 10-Hz pulsatile motor output during active exploration of textured surfaces reflects the textures' frictional properties. *J. Neurophysiol.* **122**, 922–932 (2019).
19. M. A. Thenganatt, E. D. Louis, Distinguishing essential tremor from Parkinson's disease: Bedside tests and laboratory evaluations. *Expert Rev. Neurother.* **12**, 687–696 (2012).
20. J. C. Greenland, R. A. Barker, *The Differential Diagnosis of Parkinson's Disease* (Codon Publications, 2018).
21. C. W. Hess, M. Hallett, The phenomenology of Parkinson's disease. *Semin. Neurol.* **37**, 109–117 (2017).
22. S. Tripathi, T. Arroyo-Gallego, L. Giancardo, Keystroke-dynamics for Parkinson's disease signs detection in an at-home uncontrolled population: A new benchmark and method. *IEEE Trans. Biomed. Eng.* **70**, 182–192 (2023).
23. Average number of connected devices in U.S. 2020. Statista. www.statista.com/statistics/1107206/average-number-of-connected-devices-us-house/.
24. H. Alfalahi, A. H. Khandoker, N. Chowdhury, D. Iakovakis, S. B. Dias, K. R. Chaudhuri, L. J. Hadjileontiadis, Diagnostic accuracy of keystroke dynamics as digital biomarkers for fine motor decline in neuropsychiatric disorders: A systematic review and meta-analysis. *Sci. Rep.* **12**, 7690 (2022).
25. H. M. Bronte-Stewart, L. Ding, C. Alexander, Y. Zhou, G. P. Moore, Quantitative digitography (QDG): A sensitive measure of digital motor control in idiopathic Parkinson's disease. *Mov. Disord.* **15**, 36–47 (2000).

26. L. Giancardo, A. Sánchez-Ferro, T. Arroyo-Gallego, I. Butterworth, C. S. Mendoza, P. Montero, M. Matarazzo, J. A. Obeso, M. L. Gray, R. S. J. Estépar, Computer keyboard interaction as an indicator of early Parkinson's disease. *Sci. Rep.* **6**, 34468 (2016).
27. Á. Sánchez-Ferro, M. Elshehabi, C. Godinho, D. Salkovic, M. A. Hobert, J. Domingos, J. M. T. van Uem, J. J. Ferreira, W. Maetzler, New methods for the assessment of Parkinson's disease (2005 to 2015): A systematic review. *Mov. Disord.* **31**, 1283–1292 (2016).
28. M. H. Trager, K. B. Wilkins, M. M. Koop, H. Bronte-Stewart, A validated measure of rigidity in Parkinson's disease using alternating finger tapping on an engineered keyboard. *Parkinsonism Relat. Disord.* **81**, 161–164 (2020).
29. W. R. Adams, High-accuracy detection of early Parkinson's disease using multiple characteristics of finger movement while typing. *PLOS ONE* **12**, e0188226 (2017).
30. N. Akram, H. Li, A. Ben-Joseph, C. Budu, D. A. Gallagher, J. P. Bestwick, A. Schrag, A. J. Noyce, C. Simonet, Developing and assessing a new web-based tapping test for measuring distal movement in Parkinson's disease: A Distal Finger Tapping test. *Sci. Rep.* **12**, 386 (2022).
31. O. M. J. Hooman, J. Oldfield, M. A. Nicolaou, "Detecting early Parkinson's disease from keystroke dynamics using the tensor-train decomposition" in *2019 27th European Signal Processing Conference (EUSIPCO)* (IEEE, 2019), pp. 1–5.
32. A. Milne, K. Farrahi, M. A. Nicolaou, "Less is more: Univariate modelling to detect early Parkinson's disease from keystroke dynamics" in *Discovery Science*, L. Soldatova, J. Vanschoren, G. Papadopoulos, M. Ceci, Eds. (Springer, 2018), pp. 435–446.
33. T. Arroyo-Gallego, M. J. Ledesma-Carbayo, I. Butterworth, M. Matarazzo, P. Montero-Escribano, V. Puertas-Martín, M. L. Gray, L. Giancardo, Á. Sánchez-Ferro, Detecting motor impairment in early Parkinson's disease via natural typing interaction with keyboards: Validation of the neuroQWERTY approach in an uncontrolled at-home setting. *J. Med. Internet Res.* **20**, e89 (2018).
34. Y. Zhou, X. Zhao, J. Xu, Y. Fang, G. Chen, Y. Song, S. Li, J. Chen, Giant magnetoelastic effect in soft systems for bioelectronics. *Nat. Mater.* **20**, 1670–1676 (2021).
35. National Institute for Occupational Safety and Health, *Alternative Keyboards* (U.S. Department of Health and Human Services, Centers for Disease Control and Prevention, 1997); https://stacks.cdc.gov/view/cdc/5178.
36. T. K. Ho, "Random decision forests" in *Proceedings of 3rd International Conference on Document Analysis and Recognition* (IEEE, 1995), vol. 1, pp. 278–282.
37. S.-A. Rebuffi, S. Gowal, D. A. Calian, F. Stimberg, O. Wiles, T. Mann, Data augmentation can improve robustness. arXiv:2111.05328 [cs.CV] (2021).
38. S. C. Wong, A. Gatt, V. Stamatescu, M. D. McDonnell, "Understanding data augmentation for classification: When to warp?" in *2016 International Conference on Digital Image Computing: Techniques and Applications (DICTA)* (IEEE, 2016), pp. 1–6.
39. C. Shorten, T. M. Khoshgoftaar, A survey on image data augmentation for deep learning. *J. Big Data* **6**, 60 (2019).
40. L. Torrey, J. Shavlik, L. Torrey, J. Shavlik, "Transfer learning" in *Handbook of Research on Machine Learning Applications and Trends: Algorithms, Methods, and Techniques* (IGI Global, 2010), pp. 242–264.
41. K. Weiss, T. M. Khoshgoftaar, D. Wang, A survey of transfer learning. *J. Big Data* **3**, 9 (2016).
42. F. Zhuang, Z. Qi, K. Duan, D. Xi, Y. Zhu, H. Zhu, H. Xiong, Q. He, A comprehensive survey on transfer learning. *Proc. IEEE* **109**, 43–76 (2021).
43. C. Szegedy, W. Liu, Y. Jia, P. Sermanet, S. Reed, D. Anguelov, D. Erhan, V. Vanhoucke, A. Rabinovich, "Going deeper with convolutions" in *2015 IEEE Conference on Computer Vision and Pattern Recognition (CVPR)* (IEEE, 2015), pp. 1–9.
44. N. Srivastava, G. Hinton, A. Krizhevsky, I. Sutskever, R. Salakhutdinov, Dropout: A simple way to prevent neural networks from overfitting. *J. Mach. Learn. Res.* **15**, 1929–1958 (2014).
45. Z. J. Wang, R. Turko, O. Shaikh, H. Park, N. Das, F. Hohman, M. Kahng, D. H. P. Chau, CNN explainer: Learning convolutional neural networks with interactive visualization. *IEEE Trans. Vis.* **27**, 1396–1406 (2021).
46. Z. Deng, M. J. Dapino, Review of magnetostrictive materials for structural vibration control. *Smart Mater. Struct.* **27**, 113001 (2018).
47. G. Chen, X. Zhao, S. Andalib, J. Xu, Y. Zhou, T. Tat, K. Lin, J. Chen, Discovering giant magnetoelasticity in soft matter for electronic textiles. *Matter* **4**, 3725–3740 (2021).
48. R. Atri, K. Urban, B. Marebwa, T. Simuni, C. Tanner, A. Siderowf, M. Frasier, M. Haas, L. Lancashire, Deep learning for daily monitoring of Parkinson's disease outside the clinic using wearable sensors. *Sensors* **22**, 6831 (2022).
49. S. H. Roy, B. T. Cole, L. D. Gilmore, C. J. De Luca, S. H. Nawab, "Resolving signal complexities for ambulatory monitoring of motor function in Parkinson's disease" in *2011 Annual International Conference of the IEEE Engineering in Medicine and Biology Society* (IEEE, 2011), pp. 4836–4839.
50. C. Zhong, W. W. Y. Ng, A robust frequency-domain-based graph adaptive network for Parkinson's disease detection from gait data. *IEEE Trans. Multimedia* **25**, 7076–7088 (2023).
51. F. Rodriguez, P. Krauss, J. Kluckert, F. Ryser, L. Stieglitz, C. Baumann, R. Gassert, L. Imbach, O. Bichsel, Continuous and unconstrained tremor monitoring in Parkinson's disease using supervised machine learning and wearable sensors. *Parkinsons Dis.* **2024**, 787563 (2024).

Acknowledgments: We acknowledge the Henry Samueli School of Engineering & Applied Science and the Department of Bioengineering at the University of California, Los Angeles for their startup support. We acknowledge S. Andalib for helping with the modeling analysis. **Funding:** J.C. acknowledges the Vernroy Makoto Watanabe Excellence in Research Award at the UCLA Samueli School of Engineering. This work was supported by the Office of Naval Research Young Investigator Award (award ID: N00014-24-1-2065), National Science Foundation (award number: 2425858), NIH (award ID: R01 CA287326), American Heart Association Innovative Project Award (award ID: 23IPA1054908), American Heart Association Transformational Project Award (award ID: 23TPA1141360), American Heart Association's Second Century Early Faculty Independence Award (award ID: 23SCEFIA1157587), and Caltech/UCLA joint NIH T32 Training Grant (award ID: T32EB027629). **Author contributions:** Conceptualization: T.T., G.C., J.C., and X.Z. Investigation: T.T., G.C., and J.C. Experiments: T.T., G.C., J.X., and X.Z. Methodology: T.T., G.C., J.C., J.X., and X.Z. Resources: T.T., G.C., J.C., and J.X. Data curation: T.T., G.C., J.C., and J.X. Validation: T.T., G.C., J.C., J.X., and Y.F. Formal analysis: T.T., G.C., and J.C. Software: T.T., G.C., and J.X. Visualization: T.T., G.C., X.Z., and Y.F. Funding acquisition: G.C. and J.C. Project administration: T.T., G.C., and J.C. Supervision: J.C. Writing—original draft: T.T. Writing—review and editing: T.T., G.C., J.C., and J.X. **Competing interests:** The authors declare that they have no competing interests. **Data and materials availability:** All data needed to evaluate the conclusions in the paper are present in the paper and/or the Supplementary Materials.

Submitted 6 October 2024
Accepted 28 February 2025
Published 4 April 2025
10.1126/sciadv.adt6631